SAND2022-4024C

Proceedings of the ASME 2022
Pressure Vessels & Piping Conference
PVP2022
July 17-22, 2022
Las Vegas, NV

PVP2022-83915

INVESTIGATING THE ROLE OF FERRITIC STEEL MICROSTRUCTURE AND STRENGTH IN FRACTURE RESISTANCE IN HIGH-PRESSURE HYDROGEN GAS

Joseph A Ronevich[1], Brian Kagay[1], Chris San Marchi[1]
[1]Sandia National Laboratories
Livermore, CA

Yiyu (Jason) Wang[2], Zhili Feng[2], Yanli Wang[2]
[2]Oak Ridge National Laboratory
Oak Ridge, TN

Kip Findley[3]
[3]Colorado School of Mines
Golden, CO

ABSTRACT

Despite their susceptibility to hydrogen-assisted fracture, ferritic steels make up a large portion of the hydrogen infrastructure. It is impractical and too costly to build large scale components such as pipelines and pressure vessels out of more hydrogen-resistant materials such as austenitic stainless steels. Therefore, it is necessary to understand the fracture behavior of ferritic steels in high-pressure hydrogen environments to manage design margins and reduce costs. Quenched and tempered (Q&T) martensite is the predominant microstructure of high-pressure hydrogen pressure vessels, and higher strength grades of this steel type are more susceptible to hydrogen degradation than lower strength grades. In this study, a single heat of 4340 alloy was heat treated to develop alternative microstructures for evaluation of fracture resistance in hydrogen gas. Fracture tests of several microstructures, such as lower bainite and upper bainite with similar strength to the baseline Q&T martensite, were tested at 21 and 105 MPa H_2. Despite a higher MnS inclusion content in the tested 4340 alloy which reduced the fracture toughness in air, the fracture behavior in hydrogen gas fit a similar trend to other previously tested Q&T martensitic steels. The lower bainite microstructure performed similar to the Q&T martensite, whereas the upper bainite microstructure performed slightly worse. In this paper, we extend the range of high-strength microstructures evaluated for hydrogen-assisted fracture beyond conventional Q&T martensitic steels.

NOMENCLATURE

AT	austempered
CT	compact tension
J_Q	intersection of J-R with 0.2mm construction line
K_{JIC}	plane-strain fracture toughness converted from J_Q
K_{JH}	fracture resistance in hydrogen gas converted from J_Q
K_Q	conditional fracture toughness
MnS	manganese sulfide
QT	quenched and tempered
T	tempered

1. INTRODUCTION

Quenched and tempered (Q&T) martensite is the most common microstructure in high strength pressure vessels for use in high pressure hydrogen service. The properties of Cr-Mo steels can be finely controlled by tempering the martensitic microstructure; however, the wall thickness is limited in Cr-Mo steels by its modest hardenability. Ni-Cr-Mo steels, such as 4340, provide improved hardenability, which permits the thicker wall designs that are needed for larger diameter vessels to provide improved storage capacity on a smaller footprint at lower cost.

In late 2018, ASME Code Case 2938 was approved, which permitted use of standardized fatigue crack growth rate constants (e.g., design curves) for the use with SA-372 and SA-723 steels in high-pressure construction for hydrogen applications [1, 2].

[1] Contact author: jaronev@sandia.gov

The approval of Code Case 2938 eliminated the need for in-situ hydrogen gas testing of SA-372 and SA-723 steels (Cr-Mo and Ni-Cr-Mo steels) removing a significant cost burden. In addition, it provided harmonization of the design basis through design curves based on data generated in high-pressure hydrogen. The design curves capture the behavior of the Cr-Mo and Ni-Cr-Mo data over a broad range of stress intensity factor ranges, ΔK. It was shown that design life could be improved by a factor of 3 using these design curves compared to previous design bases [3]. However, Code Case 2938 is only applicable for steels with tensile strength up to 915 MPa and maximum stress intensity factor, K_{Imax}, is not permitted to exceed 40 MPa $m^{1/2}$. These criteria come from the observation that fracture resistance in hydrogen tends to decrease significantly (e.g. to near 20 MPa $m^{1/2}$ or less) for steels with tensile strength greater than 950 MPa [1]. Here, fracture resistance is defined by the onset of subcritical crack extension as defined in ASTM E1820 [4] where the J-R curve intersects the 0.2 mm construction line as measured in gaseous hydrogen. Based on existing data, if tensile strength is limited to 915 MPa, the fracture resistance remains greater than 40 MPa $m^{1/2}$). It would be advantageous to permit steel with tensile strengths greater than 915 MPa as cost and weight savings can be achieved through thinner walls and larger storage capacity; however, current trends (Figure 1) suggest that fracture resistance would be insufficient in commonly used Q&T martensite microstructures at these high strength levels.

Before this work, limited data existed for steels tested in high-pressure hydrogen (~100 MPa pressure) with tensile strengths greater than 900 MPa, and the data that did exist were limited to Q&T martensite. Published work compared hydrogen effects on lower bainite and Q&T martensite, but the tensile strengths of these steels were above 1460 MPa and hydrogen was introduced via submersion in an acid bath [5]. The trend of fracture resistance in 100 MPa H_2 gas versus tensile strength can be observed in Figure 1, in which a significant decrease in fracture resistance is observed above 950 MPa tensile strength. As all of the steels tested in Figure 1 are Q&T martensite, it can be assumed that an inverse relationship between strength and fracture resistance exists in this high tensile strength range.

In this present study, a single 4340 (Ni-Cr-Mo) composition was heat treated to produce nine different microstructures with a range of strengths for evaluation of fracture performance in high pressure hydrogen gas. The goal was to produce and test ferritic microstructures other than conventional Q&T martensite and to identify the role of microstructural variations on hydrogen-assisted fracture. It should be noted that the term "ferritic" is used broadly to capture body-centered cubic (b.c.c.) crystal structures such as ferrite, bainite, and martensite as opposed to austenitic microstructures with face-centered cubic (f.c.c.) crystal structures. The Q&T martensitic microstructure appears to be bound by the behavior shown in Figure 1, therefore, examination of other ferritic microstructures could unveil a different trend and provide understanding towards the goal of improving the fracture resistance in the higher tensile strength regime (>915 MPa).

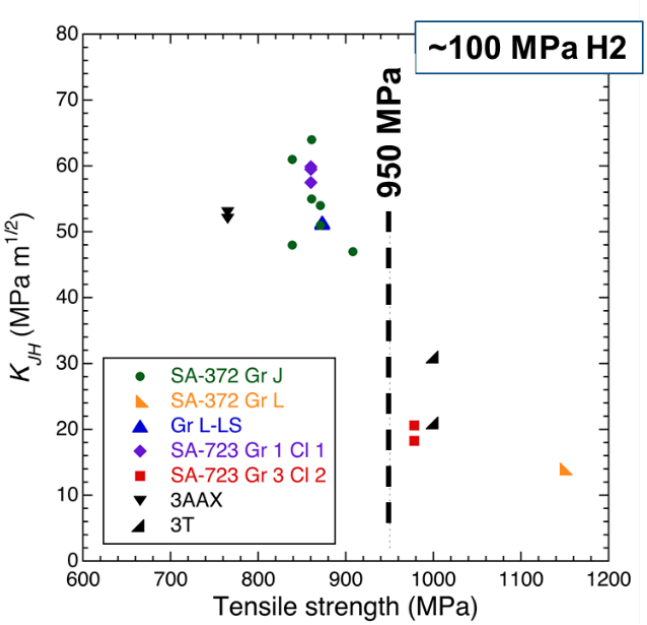

FIGURE 1: FRACTURE RESISTANCE VERSUS TENSILE STRENGTH OF QUENCHED AND TEMPERED STEEL MICROSTRUCTURES IN ~100 MPA HYDROGEN GAS. FIGURE MODIFIED FROM REF [1].

2. EXPERIMENTAL PROCEDURES

2.1 Material

The steel used in this study was a 4340 steel with the composition listed in Table 1. It should be noted that the sulfur content in this bar is 0.013 wt%, which is higher than the previous Q&T martensite steels tested in high-pressure hydrogen gas shown in Figure 1. The product came in a 44.5 mm diameter hot-rolled bar with a reduction ratio of 22:1. Tensile properties of the as-received bar were measured in the transverse direction, resulting in yield strength of 721 MPa and tensile strength of 1004 MPa. The predominant microstructural constituents are identified in Figure 2 to be ferrite, upper bainite and lower bainite. The bar was sectioned into approximately 10 mm thick slices for subsequent heat treatments.

TABLE 1 – CHEMICAL COMPOSITION OF 4340 STEEL IN WEIGHT PERCENT.

C	Mn	Si	Ni	Cr
0.405	0.714	0.259	1.751	0.822
Mo	Al	S	P	Cu
0.23	0.021	0.013	0.008	0.124

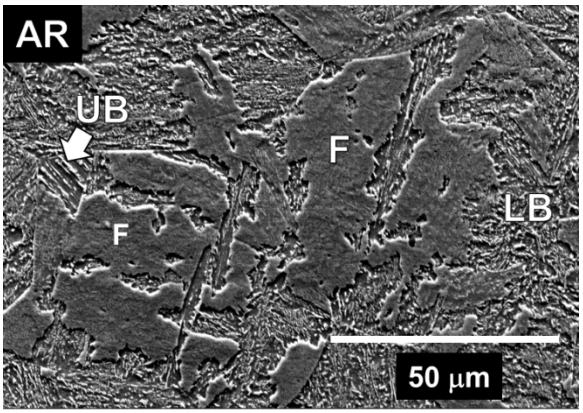

FIGURE 2: ELECTRON MICROGRAPH OF AS-RECEIVED 4340 STEEL. F=FERRITE, UB=UPPER BAINITE, LB=LOWER BAINITE.

2.2 Heat treatments

Heat treatments were conducted at Oak Ridge National Laboratory using box furnaces and each blank underwent a 30-minute austenitizing treatment at 850 °C. The subsequent thermal treatments differed to create an additional 8 microstructures for subsequent fracture testing in hydrogen gas.

Table 2 shows a summary of the heat treatment procedures as well as the measured mechanical properties and predominant microstructures resulting from the heat treatments. Figure 3 shows electron microscope images of the different heat-treated microstructures. The sample IDs are listed and were selected as convenient abbreviations of the heat treatments. For example, AT410-T460 was AusTempered at 410 °C followed by Tempering at 460 °C. The samples are listed in Table 2 in increasing tensile strength.

As Table 2 shows, the heat treatments resulted in tensile strengths ranging from 874 MPa to 1287 MPa, which correspond to Rockwell Hardness C values from 28 to 40. The temperature of the final tempering had the most pronounced effect on the hardness or strength of the material with higher tempering temperature resulting in lower strength. Therefore, although most of the heat treatments underwent final tempering, the degree to which the bainite or martensite was tempered varied. Q&T650 heat treatment was produced to create a baseline quenched and tempered martensite for comparison with relatively low strength as commonly employed for pressure vessels.

Following heat treatment on the sliced bar sections, tensile and compact tension (CT) samples were machined such that the loading axis was in the transverse direction. Tensile properties were measured on tensile samples with a gauge section diameter of 2.9 mm and a gauge section length of 15.9 mm. Tensile tests were performed in air at a displacement rate of 0.25 mm/min and yield strength was measured via the 0.2% offset intersection. Compact tension samples were machined such that the load was in the transverse direction and the crack propagated perpendicular, in the radial direction. Specimen dimensions for the CTs were width of W = 26.4 mm, machined notch depth of a/W=0.2, thickness of B = 9.5 mm, machined side grooves to reduce the net thickness to B_N = 8 mm and other dimensional ratios consistent with ASTM E1820 [4]. Prior to fracture testing, a crack was extended from the notch via fatigue testing in air or hydrogen where the final stress intensity factor, $K_{max,final}$, was less than 13 MPa $m^{1/2}$. This procedure is commonly employed to take advantage of the common test geometry for fatigue and fracture and reduce set up effort for testing in gaseous hydrogen.

2.3 Fracture testing

Displacement rates were constant and monotonic, whereas crack position was monitored via direct current potential difference (DCPD) according to ASTM E1820 [4]. Tests in air were performed at an actuator displacement rate of 0.025 mm/min and tests in hydrogen gas were performed at an actuator displacement rate of 0.005 mm/min. These rates correspond to approximate elastic K loading rates (dK/dt) of 2.5 to 0.3 MPa $m^{1/2}$ min^{-1}, respectively. The elastic K loading rates vary slightly from test to test depending on dimensions and crack lengths. A clip gauge was used to measure crack mouth opening displacement. Fracture tests were terminated after peak load, when a load drop of approximately 10-20% was observed.

Fracture testing in gaseous hydrogen was performed at pressure of 21 or 105 MPa. Testing at the lower pressure (21 MPa) was generally used to evaluate the performance in gaseous hydrogen. Subsequent tests on select samples were performed in gaseous hydrogen at pressure of 105 MPa to evaluate the effects of pressure. The in-situ mechanical test system at Sandia National Laboratories can accommodate internal transducers; therefore, an internal load cell and clip gauge were present inside the pressure vessel. Prior to filling the test volume with pure hydrogen, a series of leak checks and purges were performed first with helium, then nitrogen, and finally with hydrogen; the purging steps were developed to remove air from the system, especially oxygen and moisture. Further discussion of the testing procedures can be found in [6]. The hydrogen source gas was certified with purity of 99.9999%. Gas sampling after completion of selected tests show oxygen and moisture contents routinely below 3 and 10 ppm, respectively.

Following ASTM E1820 [4], J-R curves were developed and the J_Q was determined by the intersection of the J-R curve and the 0.2 mm offset construction line. J_Q was converted to K_{JIC} according to Eq. 1 if it met the specific size dimensions enabling it to qualify as size-independent plane-strain fracture parameter according to the criteria in Eq. 2:

$$K_{JIC} = \sqrt{\frac{EJ_Q}{(1-\nu^2)}} \quad (1)$$

$$B > 10(J_H/S_Y) \text{ and } b_o > 10(J_H/S_Y) \quad (2)$$

where E is elastic modulus, ν is Poisson's ratio (0.3), B is thickness, S_Y is effective yield strength (e.g. average of yield and tensile strength), b_o is the remaining uncracked ligament and E is the elastic modulus (207 GPa).

For tests in air, the fracture toughness is designated as K_{JIC}, indicating that an elastic-plastic analysis was performed according to ASTM E1820. For tests in hydrogen, K_{JH} also indicates that value was derived from the J-R curve, where J_H is

determined by the same procedures except the measurements are made in the hydrogen environment. In this paper, fracture toughness is used to describe the fracture behavior in air (K_{JIC}), which is a materials property, whereas fracture resistance (K_{JH}) is used to describe the fracture behavior in hydrogen gas, which is dependent on the specific environment (e.g., hydrogen pressure).

TABLE 2 – HEAT TREATED MICROSTRUCTURES AND MECHANICAL PROPERTIES OF 4340 STEEL. LISTED IN ORDER OF INCREASING TENSILE STRENGTH.

Sample	Heat treatment	Hardness (HRC)	YS (MPa)	UTS (MPa)	Phase
QT650	N-850°C-30min -WQ-T650°C-120min-WQ	28 ± 1	742	874	Tempered martensite
AT320-T650	N-850°C -30min-CC-AT320°C-60min-WQ-T-650°C-60min-WQ	28 ± 1	728	889	Tempered lower bainite
AT410-T605	N-850°C -30min-CC-AT410°C-60min-WQ-T-605°C-60min-WQ	28 ± 1	741	920	Tempered upper bainite, tempered martensite
AT320-T605	N-850°C -30min-CC-AT320°C-60min-WQ-T-605°C-60min-WQ	31 ± 1	859	992	Tempered lower bainite
AR	As-received	32 ± 1	721	1004	Ferrite, bainite
N-FC	N-850°C - 30min-FC	32 ± 2	721	1059	Ferrite, bainite, martensite, retained austenite
AT410-T460	N-850°C -30min-CC-AT410°C-60min-WQ-T-460°C-60min-WQ	33 ± 1	887	1100	Tempered upper bainite, tempered martensite
AT410	N-850°C - 30min-CC-AT-410°C -60min-WQ	34 ± 2	841	1195	Bainite, martensite
AT320-T460	N-850°C -30min-CC-AT320°C-60min-WQ-T-460°C-60min-WQ	40 ± 0.4	1158	1287	Tempered lower bainite

AR=as-received, AT=austempered, N=normalized, CC= continuous cooled, WQ=water quenched, T=tempered, FC=furnace cooled, QT=quenched & tempered

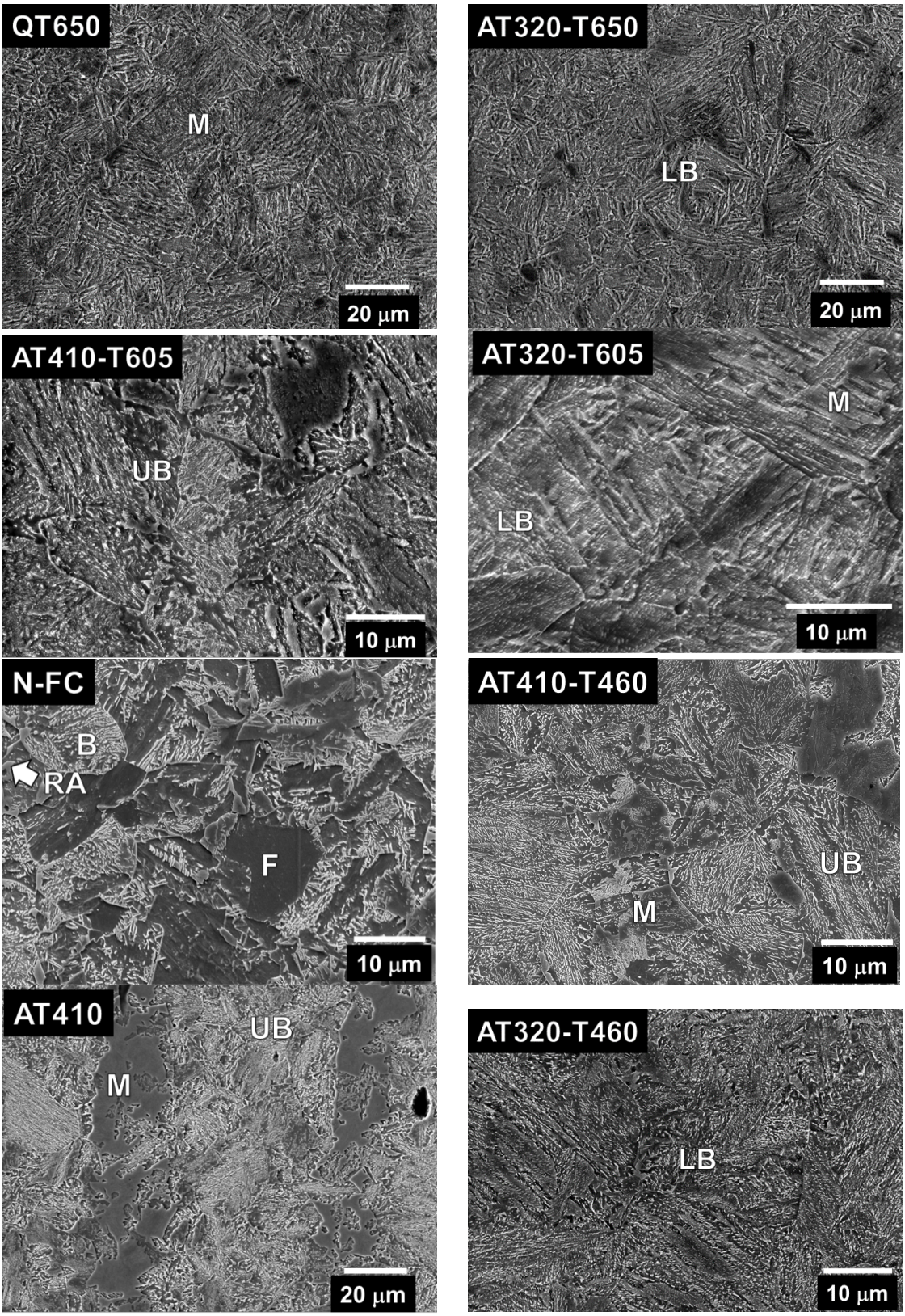

FIGURE 3: ELECTRON MICROGRAPHS OF THE 8 DIFFERENT HEAT TREATMENTS OF 4340 STEEL. THE MICROSTRUCTURES ARE IDENTIFIED AS F = FERRITE, B = BAINITE, LB = LOWER BAINITE, UB = UPPER BAINITE, RA = RETAINED AUSTENITE, M = MARTENSITE.

3. RESULTS

Fracture tests of the 8 different heat treated samples and the as-received material were performed in air and in either 21 or 105 MPa hydrogen gas. The results of the fracture tests are shown in Figure 4. All microstructures exhibited a drop in fracture resistance in hydrogen gas compared to tests in air. In air, a trend of decreasing fracture toughness is observed with increasing tensile strength up to about 1100 MPa; the fracture toughness reach a plateau for higher strength. A similar trend is apparent in hydrogen gas at pressures of both 21 and 105 MPa, where the fracture resistance decreases up to a similar strength level and then appears to plateau. The high-strength plateau of fracture resistance in hydrogen is between 20-30 MPa $m^{1/2}$, significantly lower than in air (about 50 MPa $m^{1/2}$). The effect of hydrogen pressure was evaluated on select samples (e.g., QT650 and AT320-T650) and showed a measurable decrease in fracture resistance for hydrogen at pressure 105 MPa compared to pressure of 21 MPa.

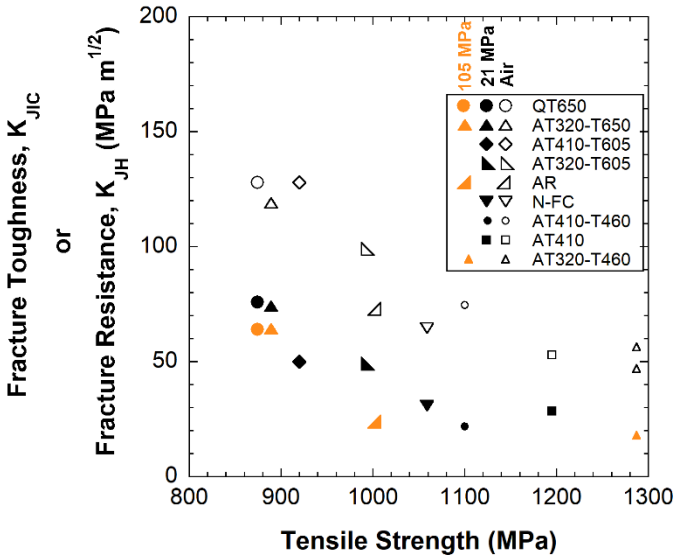

FIGURE 4: FRACTURE TOUGHNESS (K_{JIC}) OR FRACTURE RESISTANCE IN HYDROGEN (K_{JH}) AS COMPARED TO TENSILE STRENGTH.

Fracture toughness of the heat treated 4340 alloy in air is compared to other pressure vessel and pipeline steel alloys in a similar strength range in Figure 5. The 4340 heat treated samples examined in this study clearly show a lower fracture toughness compared to other alloys across the full range of strength.

Figure 6 shows fracture surfaces from fracture toughness testing in air of one of the 4340 heat treated samples (AT320-T650) and of a quench and tempered martensite pressure vessel steel (34CrMo4). The AT320-T650 fracture surface features significant amounts of elongated MnS inclusions (confirmed by electron dispersive spectroscopy, EDS), whereas the 34CrMo4 does not. Both fracture surfaces show ductile void coalescence; however, the 34CrMo4 shows more uniformity in voids throughout the fracture surface whereas the AT320-T650 shows regions of tearing near the MnS inclusions. All the fracture surfaces of the heat treated 4340 steel show similar features when tested in air.

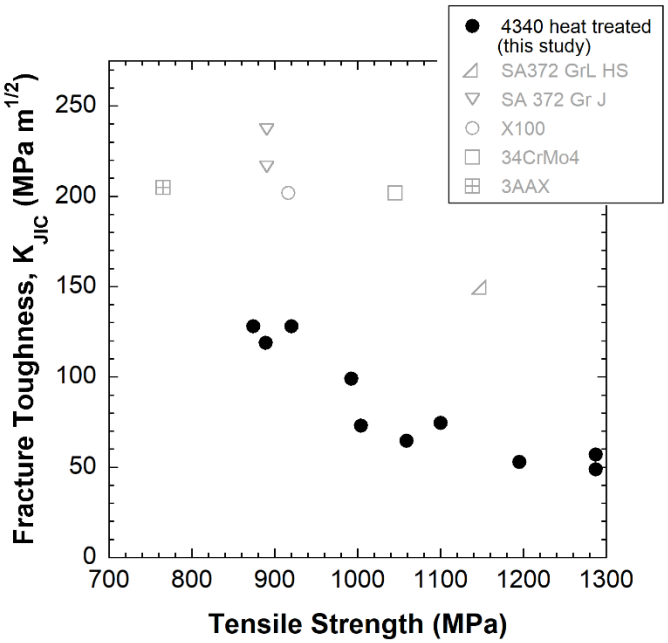

FIGURE 5: FRACTURE TOUGHNESS (K_{JIC}) OF 4340 HEAT TREATED FROM CURRENT STUDY COMPARED TO OTHER HIGH STRENGTH PRESSURE VESSEL AND PIPELINE STEELS OF SIMILAR STRENGTH ALL TESTED IN AIR.

Figure 7 shows fracture surfaces of two 4340 heat treated conditions (QT650 and AT320-T460) tested in high pressure hydrogen gas. The QT650 was tested in 21 MPa H_2 gas and the AT320-T460 was tested in 105 MPa H_2 gas. These two heat treatments represent the lower and upper bounds of strength that were produced in this study. Both fracture surfaces have a large quantity of elongated MnS inclusions. The QT650 exhibits quasi-cleavage features that are on the same scale as the martensite laths and packets, whereas the AT320-T460 exhibits more intergranular features consistent with the approximate prior austenite grain size.

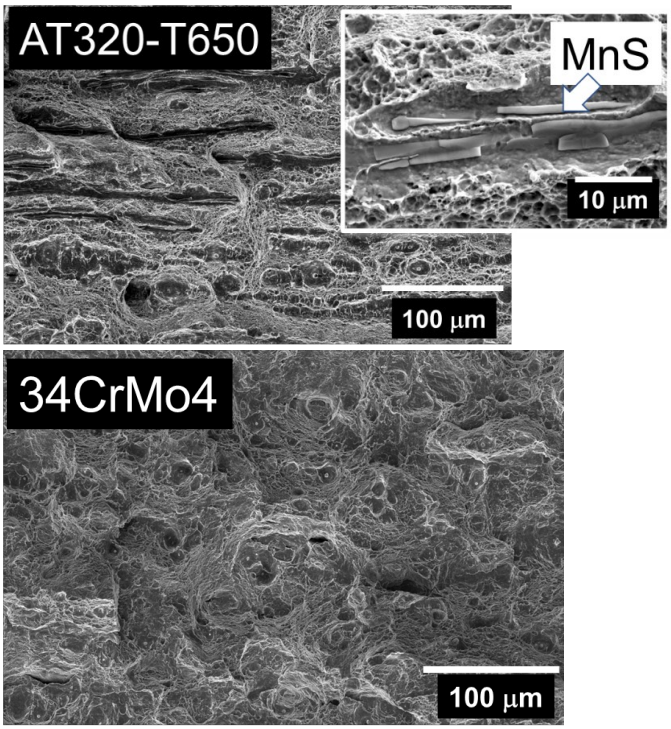

FIGURE 6*:* FRACTURE SURFACES OF FRACTURE TESTS IN AIR FOR AT320-T650 AND 34CRMO4. LARGE, ELONGATED MNS INCLUSIONS ARE OBSERVABLE ON AT320-T650 FRACTURE SURFACE. CRACK PROPAGATION DIRECTION WAS FROM BOTTOM TO TOP OF IMAGES.

4. DISCUSSION

4.1 Role of Microstructure vs Strength

The heat treatments of the 4340 in this study were motivated by the hypothesis that bainitic microstructures could display superior resistance to hydrogen than conventional tempered martensitic microstructures. The austempering treatments at temperature of 410 °C produced predominantly upper bainite and the treatment at 320 °C produced lower bainite. Subsequent tempering reduced the tensile strength of the material to the desired range between approximately 900 and 1200 MPa. Despite the large differences in microstructure, the fracture resistance appeared to be more dependent on strength than on microstructure.

Figure 8 shows fracture resistance values for the 4340 heat treated microstructures tested in this study compared to other alloys consisting of pressure vessel and pipeline steels of similar strength. All the data in Figure 8 were from tests in gaseous hydrogen at either pressure of 21 MPa or pressure greater than 100 MPa (typically 103 to 106 MPa). A best fit trendline for each pressure regime (21 or ~100 MPa) is shown.

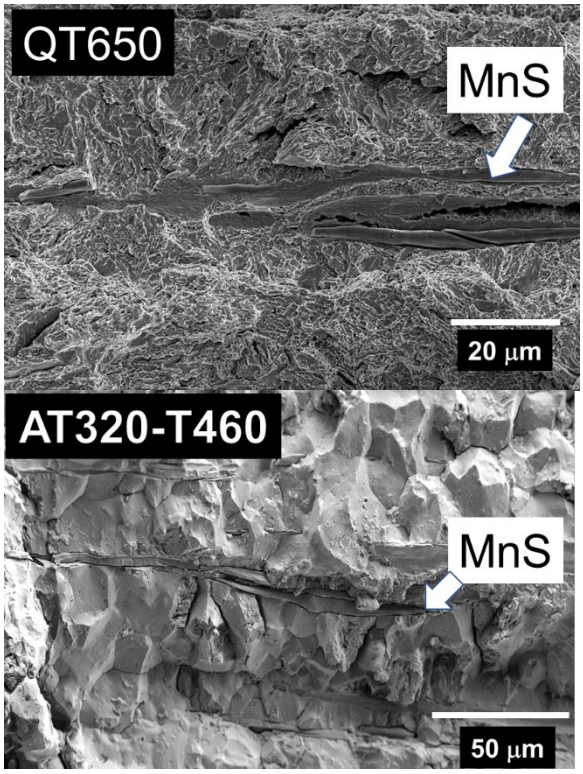

FIGURE 7: FRACTURE SURFACES OF FRACTURE TESTS IN HYDROGEN GAS FOR QT650 (21 MPA H_2) AND AT320-T460 (105 MPA H_2). ELONGATED MNS INCLUSIONS ARE PREVALENT ON BOTH FRACTURE SURFACES. CRACK PROPAGATION DIRECTION WAS FROM BOTTOM TO TOP OF IMAGES.

The general trend lines in Figure 8 show that the bainitic steels fall on the same trendlines as the martensitic steels. The data show a sharp decrease in fracture resistance in hydrogen as the tensile strength increases above 900 MPa. At higher strength, the fracture resistance in hydrogen appears to plateau. It is interesting to note that the fracture resistance appears to be independent of tensile strength between 1100 and 1300 MPa; however, it is highly unlikely that a material with K_{JH} values as low as 20 MPa $m^{1/2}$ would be selected for use in a hydrogen pressure vessel.

No difference in fracture resistance in hydrogen was observed between lower bainitic and martensitic microstructures as demonstrated by comparing fracture toughness values for materials QT650 and AT320-T650 (Figure 8). The QT650 is a tempered martensite with a tensile strength of 874 MPa. The AT320-T650 is a tempered lower bainite microstructure with a tensile strength of 889 MPa. Both materials feature Rockwell hardness values of 28 HRC, nearly identical tensile strengths and similar fracture resistance in hydrogen, yet distinct microstructures. In hydrogen gas at pressure of 105 MPa, the fracture resistance was the same for these two microstructures at 64 MPa $m^{1/2}$, whereas at pressure of 21 MPa, their fracture resistance differed by less than 3%. This similarity suggests that

the differences between lower bainite and martensite microstructures do not significantly affect fracture resistance in hydrogen.

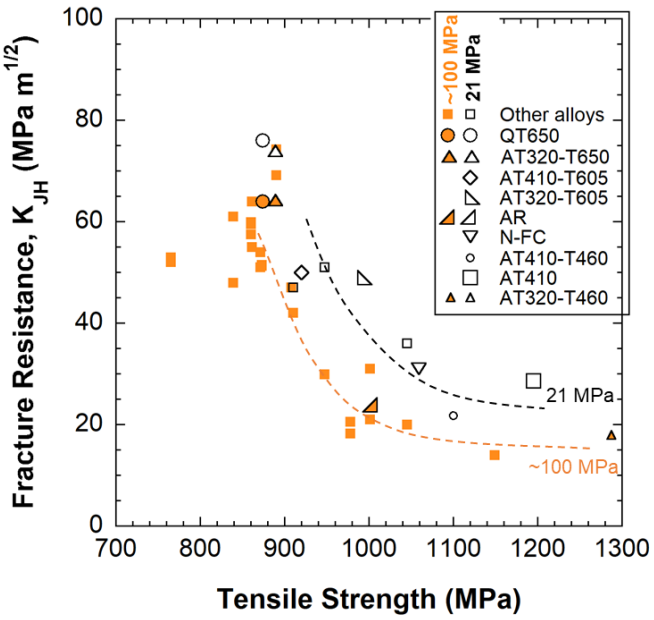

FIGURE 8: FRACTURE RESISTANCE AS A FUNCTION OF TENSILE STRENGTH FOR STEELS TESTED IN EITHER 21 MPA HYDROGEN GAS (OPEN SYMBOLS) OR ~100 MPA HYDROGEN GAS (CLOSED SYMBOLS). THE DATA FROM THIS STUDY IS PLOTTED AGAINST OTHER ALLOYS [1] CONSISTING OF PRESSURE VESSEL AND PIPELINE STEELS. BEST FIT TRENDLINES ARE SHOWN.

In the higher strength range in gaseous hydrogen at pressure of 21 MPa, AT320-T605 (tempered lower bainite) shows nearly identical fracture resistance (e.g. ~50 MPa m$^{1/2}$) compared to AT410-T605 (tempered upper bainite). The strengths of these two microstructures, however, differ. Thus, AT320-T605 falls above the 21 MPa trendline (higher strength), whereas the AT410-T605 falls below this trendline (lower strength). These two heat treatments utilized a relatively low tempering temperature (605 ˚C), which allowed them to retain higher tensile strengths of 992 MPa and 920 MPa for the AT320-T605 and AT410-T605, respectively, compared to the tempering temperature of 650˚C for the baseline Q&T microstructure. Interestingly, the fracture toughness of these two alloys in air differs quite substantially at 128 MPa m$^{1/2}$ and 99 MPa m$^{1/2}$ for the AT410-T605 and AT320-T605, respectively. This difference in relative fracture resistance between hydrogen and air demonstrates that behavior in air does not necessarily predict behavior in hydrogen. The AT320-T605 microstructure achieved fracture resistance of ~50 MPa m$^{1/2}$ for tensile strength of nominally 1000 MPa; a promising result, but further testing is needed, particularly at the desired pressure of ~100 MPa, relevant to high-pressure hydrogen storage vessels.

4.2 Role of Inclusions

Large quantities of MnS inclusions were observed on the heat treated 4340 fracture surfaces as shown in Figure 6 and Figure 7 regardless of the test environments (e.g., both in air and in hydrogen). The sulfur content in the 4340 alloy is 0.013 wt.%, which resulted in an abundance of MnS stringers in the rolled bar. For reference, the standard for ASTM A372 Grade J [7] (a common grade of Cr-Mo steels) has a stated max sulfur content of 0.01 wt.%. Furthermore, the sulfur content of the 4340 alloy was greater than many of the other tested alloys [1] in Figure 8; for these alloys, the highest reported sulfur content was 0.007 wt.%. The orientation of the CT samples with respect to the rolled bar and elongated MnS is shown in Figure 9. The MnS inclusions are elongated parallel to the crack front, thus they are visible on the 4340 alloys fracture surfaces and oriented orthogonal to the nominal crack growth direction. In contrast, the lower sulfur contents in the other alloys resulted in lower concentration of MnS inclusions and are generally absent on the fracture surfaces.

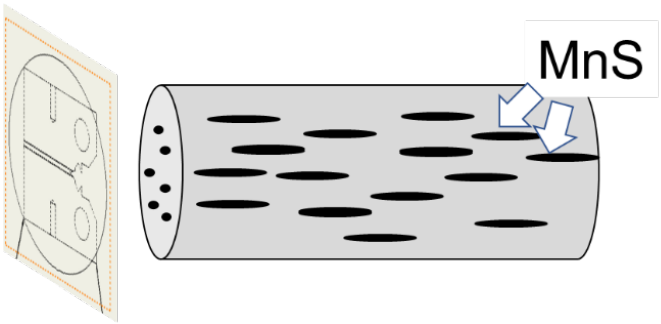

FIGURE 9: SCHEMATIC 4340 ROLLED BAR SHOWING ORIENTATION OF MNS STRINGERS AND ORIENTATION OF CT SAMPLE.

Despite the large quantity of MnS inclusions on the fracture surfaces, it appears that the inclusions have a more significant influence on fracture behavior in air than in hydrogen. All of the heat treated 4340 samples exhibited significantly lower fracture toughness in air (30-50% lower on average) compared to other pressure vessel and pipeline steels of similar strength, as shown in Figure 5. It is likely that the inclusions were the cause for this reduction in fracture toughness in air. Whereas ductile void coalescence was common to both the 4340 and other alloys as shown in Figure 6, the inclusions appear to participate in the fracture process. One interpretation is that void nucleation initiates at the MnS inclusions and linkage of these voids into a crack occurs at a lower strain due to their abundance and proximity in the 4340 alloy. The result is lower fracture toughness (in air) of the inclusion-containing material compared to the other alloys. In Figure 8, the fracture resistance values (in hydrogen) of the heat treated 4340 samples is similar to the other alloys. The data from tests performed in ~100 MPa hydrogen is the clearest example of this trend, as the values for the inclusion-containing microstructures fall at or above the trendline. Therefore, it appears that there is a strong influence of inclusions on fracture toughness in air, but minimal influence in hydrogen. When the 4340 alloys were tested in hydrogen gas, the fracture

features for the QT650 and AT320-T460, shown in Figure 7, consist of quasi-cleavage and intergranular fracture, respectively. It could be that the inclusions directly participate in the predominantly ductile fracture process in air (i.e., microvoid coalescence), but the inclusions are not involved in the less ductile process of hydrogen-assisted fracture. Their presence on the fracture surface of the tests in hydrogen may be incidental due to their abundance in the 4340 alloys. A similar quantitative trend was observed for a X52 vintage weld: the weld showed relatively poor fracture toughness in air, whereas fracture resistance in hydrogen was similar to 'clean' modern steels of the same grade and with much higher fracture toughness in air [8].

4.3 Role of Pressure

Two of the 4340 heat treated samples were tested in both 21 and 105 MPa hydrogen gas. There was a small but measurable reduction in fracture resistance at higher pressure. Fracture resistance, K_{JH}, was reduced from 76 to 64 MPa $m^{1/2}$ in QT650 and from 74 to 64 MPa $m^{1/2}$ in AT320-T650 as pressure of the gaseous hydrogen was increased from 21 to 105 MPa. As single tests were run in most of these heat treatments, it is hard to characterize the uncertainty; however, to expand the comparison of pressure effects, the trendlines in Figure 8 were drawn which show a distinct and consistent effect of pressure across the entire tested strength range. Several of the pressure vessel and pipeline steels from the literature were tested in both 21 and ~100 MPa hydrogen gas exhibiting reduction of K_{JH} between 5 and 20 MPa $m^{1/2}$ when tested at higher pressures compared to 21 MPa. Therefore, pressure does appear to reduce the fracture resistance across all the tested alloys, but this is much less than the initial decrease in fracture resistance between air and hydrogen at pressure of 21 MPa.

5. CONCLUSIONS

Nine different microstructures were produced from a single 4340 alloy by subjecting the alloy to austemper and/or quench and temper heat treatments to achieve tensile strengths between 874 and 1287 MPa. Fracture tests were performed in either gaseous hydrogen at pressure of 21 or 105 MPa to measure the fracture resistance (K_{JH}) of different microstructures of upper and lower bainite compared to martensite. All the samples tested in hydrogen gas exhibited degradation of fracture resistance. Higher pressure hydrogen tests (e.g. 105 MPa) resulted in small, but measurable, decreases in fracture resistance compared to 21 MPa hydrogen gas. It was observed that the tested alloy had a large concentration of MnS inclusions, which were prevalent on the fracture surfaces. Interestingly, the inclusions appeared to only degrade the fracture toughness in air, while having negligible effects on fracture resistance in hydrogen environments. This conclusion was reached by comparing the trends of the heat treated 4340 samples to other pressure vessel and pipeline steels with similar strengths in both air and hydrogen. The inclusions are hypothesized to directly participate in the void coalescence process for tests in air, explaining the lower fracture toughness of these microstructures compared to the alloys with lower inclusion contents. However, the high MnS inclusion content in the 4340 alloy did not appear to affect the fracture resistance in hydrogen, as comparable K_{JH} values were measured in alloys containing lower sulfur content. This observation suggests that that the MnS inclusions do not directly contribute to the predominant fracture process (e.g. quasi-cleavage or intergranular fracture) when tested in hydrogen gas. Finally, fracture resistance in hydrogen gas was quantitatively consistent among the examined bainitic microstructures compared to the trends for conventional quenched and tempered martensite, suggesting that the dominant factor in determining fracture resistance is tensile strength. It is worth noting that the tempered upper bainite microstructure (AT410-T605) showed lower fracture resistance than the general trend, suggesting poorer performance than the other bainitic and martensitic microstructures.

ACKNOWLEDGEMENTS

Sandia National Laboratories is a multi-mission laboratory managed and operated by National Technology and Engineering Solutions of Sandia, LLC., a wholly owned subsidiary of Honeywell International, Inc., for the U.S. Department of Energy's National Nuclear Security Administration under contract DE-NA-0003525. This work is supported by the U.S. Department of Energy, through the Office of Energy Efficiency and Renewable Energy's (EERE) Hydrogen and Fuel Cell Technologies Office (HFTO). *Any subjective views or opinions that might be expressed in the paper do not necessarily represent the views of the U.S. Department of Energy or the United States Government.*

REFERENCES

[1] C. San Marchi, J. Ronevich, P. Bortot, Y. Wada, J. Felbaum, and M. Rana, "Technical basis for master curve for fatigue crack growth of ferritic steels in high-pressure gaseous hydrogen in ASME Section VIII-3 code PVP2019-93907," presented at the Proceedings of the ASME 2019 Pressure Vessels & Piping Conference, San Antonio, TX, July 14-19, 2019. doi:10.1115/PVP2019-93907

[2] *Code Case 2938 Hydrogen crack growth rate constants, threshold stress intensity factor KIH, and critical crack size requirementes for SA-372 and SA-723 Steels Section VIII, Division 3*, A. BPVC, December 19, 2018.

[3] J. Ronevich, C. San Marchi, D. Brooks, J.M. Emery, P. Grimmer, E. Chant, J. Robert Sims, A. Belokobylka, D. Farese, J. Felbaum, "Exploring life extension opportunities of high-pressure hydrogen tanks at refueling stations PVP2021-61815," in *ASME 2021 Pressure Vessels & Piping Conference*, Virtual, ASME, Ed., 2021, doi:10.1115/PVP2021-61815.

[4] *E1820-18a Standard Test Method for Measurement of Fracture Toughness*, ASTM, West Conshohocken, PA, 2018.

[5] J. M. Tartaglia, K. A. Lazzari, G. P. Hui, and K. L. Hayrynen, "A Comparison of Mechanical Properties and Hydrogen Embrittlement Resistance of Austempered vs Quenched and Tempered 4340 Steel," *Metallurgical and Materials Transactions A,* 39 (2008) pp. 559-576, doi: 10.1007/s11661-007-9451-8.

[6] B. P. Somerday, J. A. Campbell, K. L. Lee, J. A. Ronevich, and C. San Marchi, "Enhancing safety of hydrogen containment components through materials testing under in-service conditions," *International Journal of Hydrogen Energy,* 42 (2017) pp. 7314-7321, doi: 10.1016/j.ijhydene.2016.04.189.

[7] *Standard Specification for Carbon and Alloy Steel Forgings for Thin-Walled Pressure Vessels*, ASTM, 2020.

[8] J. A. Ronevich, E. J. Song, B. P. Somerday, and C. W. San Marchi, "Hydrogen-assisted fracture resistance of pipeline welds in gaseous hydrogen," *International Journal of Hydrogen Energy* 46 (2021) pp. 7601-7614, doi:10.1016/j.ijhydene.2020.11.239.